JOURNAL OF PROPULSION AND POWER
Vol. 9, No. 3, May–June 1993

Computations and Experiments for a Multiple Normal Shock/Boundary-Layer Interaction

B. F. Carroll* and P. A. Lopez-Fernandez†
University of Florida, Gainesville, Florida 32611
and
J. C. Dutton‡
University of Illinois at Urbana-Champaign, Urbana, Illinois 61801

Results from a numerical investigation of a Mach 1.61 multiple normal shock wave/turbulent boundary-layer interaction are compared to wall static pressure and laser Doppler velocimeter measurements. The computations used the explicit, time-dependent, second-order accurate MacCormack scheme to solve the mass-averaged Navier-Stokes equations. Turbulence was modeled by means of the Baldwin-Lomax algebraic model and the Wilcox-Rubesin two-equation model. The computation with the Wilcox-Rubesin model was able to capture the major features of the normal shock train and accurately predicted the flow reacceleration mechanisms which occur between shocks. However, this computation failed to accurately predict the level of flow separation under the first shock. The Baldwin-Lomax computation displayed a more limited ability to capture the features of this shock train flow.

Nomenclature

A^+ = constant in Baldwin-Lomax model
C_{cl} = Clauser constant
C_{cp} = constant in Baldwin-Lomax model
C_{kleb} = constant in Baldwin-Lomax model
$F_{kleb}(y)$ = Klebanoff intermittency function
H = stagnation enthalpy
h = static enthalpy
J = Jacobian of the coordinate transformation
k = turbulence kinetic energy
P = static pressure
Pr = Prandtl number
R = gas constant
Re = Reynolds number
T = static temperature
t = time
u = streamwise velocity component
v = transverse velocity component
x = streamwise direction in physical space
y = transverse direction in physical space
β^* = constant in the Wilcox-Rubesin model
ζ = vorticity
η = streamwise coordinate in computational space
κ = von Karman's constant
μ = viscosity
ξ = transverse coordinate in computational space
ρ = density
σ = normal stress
σ^* = constant in the Wilcox-Rubsin model
τ = shear stress
ω = specific turbulence dissipation

Subscripts
e = edge of the boundary layer
l = laminar
t = turbulent
u = undisturbed location at the start of the pressure rise
0 = stagnation location

Superscripts
l = laminar
t = turbulent

Introduction

WITH the renewed interest in supersonic and hypersonic air breathing propulsion, the ability to compute flowfields with highly confined shock wave/turbulent boundary-layer interactions is increasingly important. Such flows commonly occur in ramjet and scramjet inlets as well as in other devices such as supersonic ejectors and supersonic diffusers. The level of flow confinement, as described by the ratio of the undisturbed boundary-layer thickness to the duct half height, δ_u/h, is known to exert a strong influence on the interaction.[1-3] This article focuses on the highly confined multiple normal shock wave/turbulent boundary-layer interaction, or normal shock train, in a nearly constant area, rectangular duct. Numerical simulations of the normal shock train were performed using the explicit MacCormack scheme[4] to integrate the time-dependent, mass-averaged Navier-Stokes equations along with the two-equation Wilcox-Rubesin[5] model of turbulence and the algebraic Baldwin-Lomax[6] turbulence model. This approach is typical of those currently being used for scramjet engine analysis as discussed by White et al.[7] Comparisons to detailed wall static pressure and velocity measurements in a normal shock train[8,9] are used to evaluate the accuracy of the numerical predictions. To the authors' knowledge, the results presented here are the first reported computations of a normal shock train and the only detailed comparison of such computations to LDV measurements.[10] Subsequent computations of shock train flows have appeared in recent years, reflecting the renewed interest in this topic,[11-13] although these recent computations have not generally focused on the detailed mechanisms of the shock/boundary-layer interactions.

Received April 10, 1992; revision received Dec. 8, 1992; accepted for publication Dec. 11, 1992.

*Assistant Professor, Department of Aerospace Engineering, Mechanics and Engineering Science. Member AIAA.
†Graduate Assistant, Department of Aerospace Engineering, Mechanics and Engineering Science. Student Member AIAA.
‡Professor, Department of Mechanical and Industrial Engineering. Associate Fellow AIAA.

Numerous researchers have applied numerical techniques for solving the mass-averaged Navier-Stokes equations to both unconfined and confined shock wave/turbulent boundary-layer interactions. The work cited here is not intended to be a comprehensive list of the related work; only some of the most closely related work is discussed. The first reported computation of a bifurcated shock pattern at the interaction of a normal shock with a turbulent boundary layer is given by Liou et al.[14] These computations accurately captured the shock location and lambda structure in two diverging ducts with area ratios of 1.52 and 2.37. Using a similar formulation, Om et al.[1] present numerical and experimental results for a normal shock wave/turbulent boundary-layer interaction in a constant area circular duct. The confinement levels were sufficiently low that only a single normal shock was observed. The computations captured the bifurcated shock structure and the supersonic tongue following the bifurcation. They employed the Wilcox-Rubesin turbulence model which has been found to perform well in these types of flows.[15] Other researchers have proven the ability of shock-capturing techniques employing some form of MacCormack's finite-difference method[4] to compute single terminal normal shocks and reflected oblique shocks in supersonic inlet flows.[16-20] Based on these previous results, the formulation used in this research is reasonable.

Formulation

The supersonic diffuser simulation, version 1 (SUDS1) computer code used in this work is based on the NASCRIN code developed by Kumar.[17] The major differences are that a reference plane characteristic-type outflow boundary condition, wall function boundary conditions, and the two-equation Wilcox-Rubesin turbulence model have been incorporated into SUDS1. The governing equations for the mean flow are the same as those used by Kumar,[16,17] i.e., the conservation form of the two-dimensional, planar, mass-averaged, time-dependent Navier-Stokes equations. A coordinate transformation, from the (x, y) physical space to the (ξ, η) computational space, is applied such that the equations remain in strong conservation form. The resulting equations are

$$\frac{\partial \boldsymbol{U}}{\partial t} + \frac{\partial \boldsymbol{M}}{\partial \xi} + \frac{\partial \boldsymbol{N}}{\partial \eta} = 0 \tag{1}$$

where the vectors $\boldsymbol{U}$, $\boldsymbol{M}$, and $\boldsymbol{N}$ are

$$\boldsymbol{U} = J \begin{bmatrix} \rho \\ \rho u \\ \rho v \\ \rho H - P \end{bmatrix} \tag{2}$$

$$\boldsymbol{M} = \begin{bmatrix} \rho\bar{u} \\ \rho u\bar{u} + y_\eta \sigma_x - x_\eta \tau_{xy} \\ \rho v\bar{u} + y_\eta \tau_{xy} - x_\eta \sigma_y \\ \rho H\bar{u} - P\bar{u} + y_\eta(u\sigma_x + q_x) - x_\eta(v\sigma_y + q_y) \\ + \tau_{xy}(vy_\eta - ux_\eta) \end{bmatrix} \tag{3}$$

$$\boldsymbol{N} = \begin{bmatrix} \rho\bar{v} \\ \rho u\bar{v} - y_\xi \sigma_x + x_\xi \tau_{xy} \\ \rho v\bar{v} - y_\xi \tau_{xy} + x_\xi \sigma_y \\ \rho H\bar{v} - P\bar{v} - y_\xi(u\sigma_x + q_x) + x_\xi(v\sigma_y + q_y) \\ + \tau_{xy}(-vy_\xi + ux_\xi) \end{bmatrix} \tag{4}$$

with

$$\bar{u} = (y_\eta u - x_\eta v) \tag{5}$$

$$\bar{v} = (-y_\xi u + x_\xi v) \tag{6}$$

The Jacobian of the transformation is given as $J = x_\xi y_\eta - x_\eta y_\xi$, and the metrics of the transformation are defined as $y_\eta = \xi_x J$, $x_\eta = -\xi_y J$, $y_\xi = -\eta_x J$, and $x_\xi = \eta_y J$.

The total stress tensor is defined by $\tau_{ij} = \tau^l_{ij} + \tau^t_{ij}$, with the laminar stresses given by

$$\tau^l_{ij} = -\mu_l \left(\frac{\partial u_i}{\partial x_j} + \frac{\partial u_j}{\partial x_i} \right) + \frac{2}{3} \delta_{ij} \left(\mu_l \frac{\partial u_k}{\partial x_k} + P \right) \tag{7}$$

and the turbulent stresses obtained from

$$\tau^t_{ij} = -\mu_t \left(\frac{\partial u_i}{\partial x_j} + \frac{\partial u_j}{\partial x_i} \right) + \frac{2}{3} \delta_{ij} \left(\mu_t \frac{\partial u_k}{\partial x_k} + \rho k \right) \tag{8}$$

The total heat flux is also made up of a laminar and turbulent contribution

$$q_x = -\left(\frac{\mu_l}{Pr_l} + \frac{\mu_t}{Pr_t} \right) \frac{\partial h}{\partial x} \tag{9}$$

$$q_y = -\left(\frac{\mu_l}{Pr_l} + \frac{\mu_t}{Pr_t} \right) \frac{\partial h}{\partial y} \tag{10}$$

The laminar viscosity μ_l is obtained from the Sutherland viscosity law. The laminar and turbulent Prandtl numbers for air are taken as $Pr_l = 0.72$ and $Pr_t = 0.90$, respectively. In the energy equation, the dependent variable is written as $\rho H - P$, and is physically interpreted as the total internal energy per unit volume. One additional relation, beyond the turbulence model for μ_t, is required to close this set of equations. This is taken as the ideal gas law $P = \rho RT$.

The turbulent viscosity is modeled by $\mu_t = \rho V_t L_t$, where V_t and L_t are characteristic velocity and length scales of the turbulent flow. The two turbulence models employed in this investigation, one due to Baldwin and Lomax[6] and the other to Wilcox and Rubesin,[5] are used to compute the turbulent viscosity. The Baldwin-Lomax model has the advantages of easy implementation and efficient execution and has been used successfully for flows with small separations. The two-equation models are generally better than algebraic models for shock/boundary-layer interactions, but they still have difficulty predicting the mean flow features without adjusting the parameters of the model.

The widely used Baldwin-Lomax model[6] is a two-layer, algebraic, isotropic eddy viscosity turbulence model. The turbulent viscosity is calculated using separate formulations in each of two distinct layers, the inner layer close to a solid wall, and the outer layer away from the wall. A smooth transition between the two formulations is enforced as follows:

$$\mu_t = \begin{cases} (\mu_t)_{\text{inner}} & y \le y_{\text{crossover}} \\ (\mu_t)_{\text{outer}} & y_{\text{crossover}} < y \end{cases} \tag{11}$$

Here, y is the normal distance from the wall, and the crossover point is the closest location to the wall at which the outer and inner turbulent viscosities are equal. In the inner region, the Prandtl-van Driest formulation is used

$$(\mu_t)_{\text{inner}} = \rho L_t^2 |\zeta| \tag{12}$$

where the turbulent length scale is $L_t = \kappa_y D$, the turbulent velocity scale is $L_t|\zeta|$, κ is von Karman's constant, and $|\zeta|$ is the magnitude of the vorticity

$$|\zeta| = \sqrt{\left(\frac{\partial u}{\partial y} - \frac{\partial v}{\partial x} \right)^2} \tag{13}$$

D is the van Driest damping factor, $D = [1 - \exp(-y^+/A^+)]$, and $y^+ = y\sqrt{\rho_w \tau_w}/\mu_w$. The outer turbulent viscosity is

calculated from

$$(\mu_t)_{\text{outer}} = C_{cl}C_{cp}\rho F_{\text{wake}}F_{kleb}(y) \tag{14}$$

$F_{kleb}(y)$ is given by

$$F_{kleb}(y) = [1 + 5.5(C_{kleb}y/y_{\max})^6]^{-1} \tag{15}$$

The wake function is calculated from $F_{\text{wake}} = y_{\max}F_{\max}$, where $y_{\max}$ is the y location of the peak in the function $F(y) = y|\zeta|D$ and $F_{\max} = F(y_{\max})$. The turbulent length scale in the outer region is proportional to $y_{\max}$, and the turbulent velocity scale is proportional to $F_{\max}$. Thus, the distribution of vorticity in the outer region is used to establish these outer scales. Baldwin and Lomax[6] noticed in their original paper that the function $F(y)$ can develop multiple peaks in the vicinity of a shock wave/boundary-layer interaction. If the wrong peak is selected, the function F_{wake} will be incorrectly evaluated. Visbal and Knight[21] investigated this effect in more detail. Their results indicated that two main peaks develop in the separation region of a shock wave/boundary-layer interaction. Selection of the inner peak causes artificially low values of F_{wake}, while selection of the outer peak physically gave more reasonable results, leading them to recommend use of the outer peak. They also noted that near the separation point, where the wall shear stress goes to zero, the van Driest damping function unrealistically vanishes, causing low values of the computed turbulent viscosity. The use of the local shear stress, instead of the wall shear stress, avoided this problem. Visbal and Knight's[21] work also indicated that the constants C_{cp} and C_{kleb} exhibited a Mach number dependence. A value of $C_{cp} = 2.08$ was recommended for a Mach 3.0, nearly adiabatic flat-plate boundary layer, but no specific recommendation concerning C_{kleb} in a compressible flow was made. The original values of the model constants were used in the current study[6]: $A^+ = 26$, $C_{cp} = 1.6$, $C_{kleb} = 0.3$, $\kappa = 0.4$, $C_{cl} = 0.0168$. Also, the outer peak of the function $F(y)$ was selected.[21] Once μ_t is calculated, the turbulent stress tensor τ_{ij}^t is obtained from the constitutive relation [Eq. (8)], with the kinetic energy term, ρk, set to zero.

The Wilcox-Rubesin turbulence model[5] is a two-equation, eddy viscosity model. In this work, the quantity k is taken as the two-dimensional turbulence kinetic energy, i.e., $k = (\overline{u'^2} + \overline{v'^2})/2$. The specific turbulence dissipation, defined as the rate of dissipation of turbulence kinetic energy per unit of turbulence kinetic energy, is related to the dissipation of turbulence kinetic energy, by

$$\omega = (\varepsilon/\beta^* k) \tag{16}$$

where β^* is a constant. The turbulent viscosity is calculated from

$$\mu_t = \rho\gamma^*(k/\omega) \tag{17}$$

where k and ω are obtained from the turbulence model equations for ρk and $\rho\omega^2$

$$\frac{\partial(\rho k)}{\partial t} + \frac{\partial(\rho u_j k)}{\partial x_j} + \tau_{ij}^t\frac{\partial(u_i)}{\partial x_j} + \beta^*\rho\omega k - \frac{\partial}{\partial x_j}\left[(\mu_l + \sigma^*\mu_t)\frac{\partial(k)}{\partial x_j}\right] = 0 \tag{18}$$

$$\frac{\partial(\rho\omega^2)}{\partial t} + \frac{\partial(\rho u_j\omega^2)}{\partial x_j} + \gamma\frac{\omega^2}{k}\tau_{ij}^t\frac{\partial(u_i)}{\partial x_j} + \left[\beta + 2\sigma\left(\frac{\partial L_t}{\partial x_k}\right)^2\right] \cdot \rho\omega^3 - \frac{\partial}{\partial x_j}\left[(\mu_l + \sigma\mu_t)\frac{\partial(\omega^2)}{\partial x_j}\right] = 0 \tag{19}$$

The turbulent length scale is $L_t = \sqrt{k}/\omega$. Five terms appear in each of the turbulence model equations for ρk and $\rho\omega^2$. From left to right, these terms are the time rate of change followed by the convection, production, viscous dissipation, and viscous diffusion terms. A viscous damping term γ^* is included in the expression for the turbulent viscosity and is given by

$$\gamma^* = [1 - (1 - \lambda^2)\exp(-Re_t/R_k)] \tag{20}$$

To allow a different level of damping in the $\rho\omega^2$ equation, a second damping term γ is defined by

$$\gamma\gamma^* = \gamma_\infty[1 - (1 - \lambda^2)\exp(-Re_t/R_\omega)] \tag{21}$$

These viscous damping terms were required in the model to correctly simulate the near wall region where molecular viscosity dominates. The Reynolds number of turbulence is expressed as $Re_t = (\rho\sqrt{k}L_t)/\mu_l$. The original model closure coefficients[5] are: $\beta = \frac{3}{20}$, $\beta^* = \frac{9}{100}$, $\sigma = \sigma^* = \frac{1}{2}$, $\gamma_\infty = \frac{10}{9}$, $\lambda = \frac{1}{11}$, $R_k = 1$, and $R_\omega = 2.0$. Viegas and Horstman[15] found that calculations with the original value of $\gamma_\infty = \frac{10}{9}$ underpredicted the wall shear stress in a flat-plate equilibrium boundary layer by 27%, and recommended that a value of $\gamma_\infty = 0.90$ be used instead. However, Liou et al.[14] found that using the original value of $\gamma_\infty = \frac{10}{9}$ yielded separation regions at the foot of a bifurcated shock which were in better agreement with experimental data. Liou et al.[14] also recommended that the closure coefficients appearing in the viscous dissipation terms of the model equations be set to unity, $\sigma = \sigma^* = 1.0$, to give better agreement to experimental results for pressure distributions and shock locations in several calculations of the bifurcated terminal shock in a ramjet-type diffuser. Since the choice of model constants appears to be somewhat problem-dependent, the constants used in this investigation are the original model constants as given by Wilcox and Rubesin,[5] and listed above.

This set of model equations, when solved in conjunction with the mean flow equations, gives μ_t and k. In Wilcox and Rubesin's[5] original work, terms were added to the constitutive relation [Eq. (8)] to allow for nonaligned stress and strain. These terms, intended as a correction to the isotropic model for anisotropic effects, have been found to cause numerical difficulties at times,[15] especially in calculations of shock wave/boundary-layer interaction flows, and have therefore not been included in the current formulation.

Numerical Procedure and Boundary Conditions

The set of governing equations given above was solved using the original explicit, time-dependent, second-order accurate, predictor-corrector, finite-difference method of MacCormack.[4] This method has the advantages of being easily implemented and highly vectorizable. A fourth-order numerical damping option is also included in the code to avoid excessively large numerical oscillations in the computed results near the shocks.[22] The Wilcox-Rubesin turbulence model equations also tended to go unbounded near the shocks. Procedures similar to those of Coakley and Viegas[23] were used to maintain the stability of the solution in these regions.

Appropriate boundary conditions were imposed at the edges of the computational domain. The incoming flow was supersonic except in the very near wall boundary layer. Therefore, the governing equations are either hyperbolic or parabolic everywhere at the inflow boundary. Accordingly, the primitive variables u, v, T, P, k, and ω are held fixed at specified incoming values. At the symmetry boundary, the symmetric quantities u, T, P, k, and ω are obtained from a one-point extrapolation, while the antisymmetric quantity v is set to zero. At the outflow boundary, the turbulence variables k and ω are extrapolated at both supersonic and subsonic points. At supersonic outflow points, u, v, P, and T are extrapolated

as well. At subsonic outflow points, a nonreflective reference plane characteristics scheme is used to compute the values of u, v, and T at the exit plane. The value of P is specified. This subsonic outflow boundary condition is physically consistent with the method of characteristics analysis which shows that only one characteristic extends outside the computational domain. Adiabatic, no-slip, solid wall boundary conditions are enforced at the remaining boundary. With the Baldwin-Lomax model, the mean flow equations are integrated to the wall with the first grid point off the wall placed in the viscous sublayer. The u and v velocity components are set to zero, and the wall temperature is obtained from a zeroth-order extrapolation which is equivalent to enforcing a zero normal temperature gradient. When using the Wilcox-Rubesin model, the wall function boundary conditions of Viegas et al.,[24] designed for separated compressible flows, were employed. Further details of the formulation are given in the report by Carroll and Dutton.[25]

Results

The computations were performed for the planar Mach 1.61 normal-shock train shown in Fig. 1. Detailed experimental data are available for this case, including wall static pressure measurements, surface oil flow visualizations, spark schlieren photographs, and two-component laser Doppler velocimeter measurements.[8,9] The operating conditions were as follows: stagnation pressure $P_0 = 206 \pm 0.7$ kPa; stagnation temperature $T_0 = 295 \pm 2$ K; and unit Reynolds number, $Re/m = 30 \times 10^6$ m^{-1}. The undisturbed boundary-layer thickness was $\delta_u = 5.4$ mm, and the confinement level was $\delta_u/h = 0.32$. The general characteristics of shock train interactions are discussed by Carroll and Dutton.[3] Several general features of the Mach 1.61 normal shock train are apparent in Fig. 1. The first shock is bifurcated while the following secondary shocks are not. The region near the boundary-layer edge remains supersonic throughout the interaction, while the core flow goes subsonic following each shock in the system. A slip line is generated at the bifurcation point of the first shock and extends downstream through the trailing shocks. A large increase in the boundary-layer thickness occurs under the first shock. Each successive shock in the system is weaker, and the spacing between successive shocks decreases through the interaction.

Experimental data from upstream of the interaction were used for the incoming computational boundary condition. The computation was initialized by specifying the static pressure at the exit of the computational domain. One-dimensional normal shock relations were then used to obtain an approximate subsonic exit plane Mach number, and adiabatic relations were used to obtain the corresponding exit plane static temperature. The transverse exit plane velocity was set to zero and the streamwise exit plane velocity was extracted from the exit Mach number. The distributions of the turbulence quantities were assumed to be equal to the inlet values. The values of all flow properties between the inlet and exit planes were obtained from a linear interpolation, in the computational domain, between the inlet and exit.

The computational grids used for the Wilcox-Rubesin and the Baldwin-Lomax cases are given in Table 1. Taking advantage of the symmetry in the problem, only the upper half

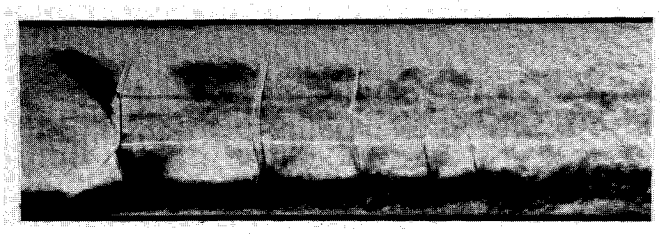

Fig. 1 Schlieren photograph of the Mach 1.61 normal shock train with flow from left to right.

Table 1 Computational grids

	Wilcox-Rubesin	Baldwin-Lomax
Streamwise domain	250 mm	753.8 mm
Streamwise grid points	117	112
Transverse grid points	55	25
First point off wall	$y^+ = 12.5$	$y^+ = 6.6$
Minimum streamwise spacing	$\Delta x/\delta_u = 0.185$	$\Delta x/\delta_u = 0.360$

of the flow was computed with the symmetry plane located at the bottom boundary. The grid for the Wilcox-Rubesin case is more highly resolved than for the Baldwin-Lomax case. A computation using the Baldwin-Lomax model and the same grid as the Wilcox-Rubesin case presented here, was reported by Carroll and Dutton,[10] but produced results inferior to the Baldwin-Lomax case, due in part to difficulty in maintaining a fixed shock location with the more highly refined grid.

The computation with the Wilcox-Rubesin turbulence model was run for a total of 70,000 iterations, which was sufficient time for a particle traveling at the incoming freestream velocity to traverse the measurement volume 8.7 times. The computational rate was 4.8×10^{-5} CPU s/grid point/iteration for a total CPU time of 6 h on a Cray X-MP. The shock train had a tendency to move downstream within the computational domain. As discussed below, the exit plane pressure was raised above the experimentally observed value to try to stabilize the shock in the duct. The shock location remained fixed for at least 10,000 iterations in the final converged solution. The mass flow rate evaluated at each streamwise location was constant to within $\pm 3\%$ over the computational domain. The maximum variation occurred in the core flow at the first shock. A grid refinement study with the Wilcox-Rubesin case was performed and showed that the solution is essentially grid independent. But, the shock train was found to move toward the exit plane as the transverse grid is refined. However, the flow structure remained essentially unchanged. Further refinements in the streamwise direction had little influence. This behavior indicates that the slope of the pressure rise is highly dependent on the transverse grid resolution.

The computation with the Baldwin-Lomax model was run for a total of 172,000 iterations. This large number of iterations for convergence was required due to the much larger physical streamwise domain in the Baldwin-Lomax case. The computational rate was 8.6×10^{-6} CPU s/grid point/iteration for a total CPU time of 1.5 h on a Cray X-MP. The Baldwin-Lomax case also showed a tendency for the shock system to move downstream in the duct, but the shock location was constant in the final converged results.

Mach number contours for the experimental results, the Wilcox-Rubesin computation and the Baldwin-Lomax computation, are shown in Fig. 2. The results have been reflected about the centerline to show the entire physical domain. Both computations failed to properly locate the shock system in the duct, so the results have been shifted to a common origin beginning at the wall static pressure rise. The Baldwin-Lomax results capture three shocks in the system with the first one bifurcated. However, the Mach number remains supersonic through the first shock. The bifurcation point in the Baldwin-Lomax case is closer to the centerline than in the experiments, possibly contributing to the failure to capture subsonic flow following the normal portion of the first shock. Insufficient streamwise grid resolution may also be a contributing factor. The spacing between the shocks is overpredicted, as is the downstream extent of the interaction. The Wilcox-Rubesin case does a better job of predicting the shock train structure. This computation captures the first, second, and third shocks in the system. The later shocks in the system are very weak. The spacing between shocks also matches the experiments well. Similar to the Baldwin-Lomax case, the Wilcox-Rubesin

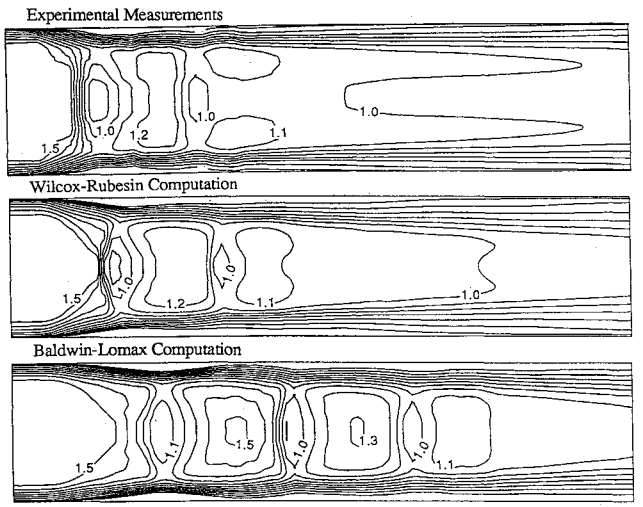

Fig. 2 Mach number contour plots M shifted for common initial pressure rise; plot range is 0.4–1.5 in increments of 0.1.

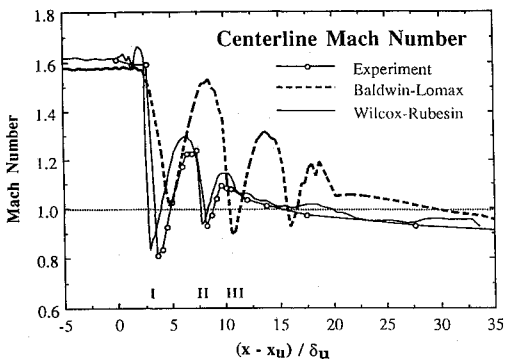

Fig. 3 Centerline Mach number distribution, shifted for common initial pressure rise. The I, II, and III denote the locations of the first, second, and third shocks, respectively.

computation locates the bifurcation points too close to the centerline. The centerline Mach number distributions are shown in Fig. 3, again shifted such that the initial wall static pressure rise coincides with the experiments. This figure emphasizes that the Wilcox-Rubesin computation does a much better job of predicting both the strength of successive shocks in the system, the magnitude of the Mach number through each shock, and the location of these shocks. The Baldwin-Lomax case captured the overall features of the shock train, but failed to give close quantitative agreement with the data.

Transverse velocity contour plots are presented in Fig. 4. Carroll and Dutton[8] discuss the significance of transverse velocity in the flow reacceleration process. The slightly oblique nature of the core part of the leading normal shock causes the transverse velocity immediately downstream of the first shock to be directed toward the centerline, forming an aerodynamic nozzle. In the near wall region, the flow under the bifurcation first turns away from the wall, then turns back toward the wall. This causes an expansion fan to form in the supersonic flow at the boundary-layer edge, which accelerates the flow in this region. Similar turning processes occur after each subsequent shock in the system. The laser Doppler velocimetry (LDV) measurements were concentrated in the regions between the first and second and between the second and third shocks. The LDV measurement resolution for shocks further downstream in the train is very coarse. As a result, the variation in the transverse velocity in the later stages of the shock train is not resolved in the experiments. The computed results with the Wilcox-Rubesin model appear to adequately predict the transverse velocity behavior, and may even overpredict the magnitude of the variations in transverse velocity through the trailing shocks. The Baldwin-Lomax

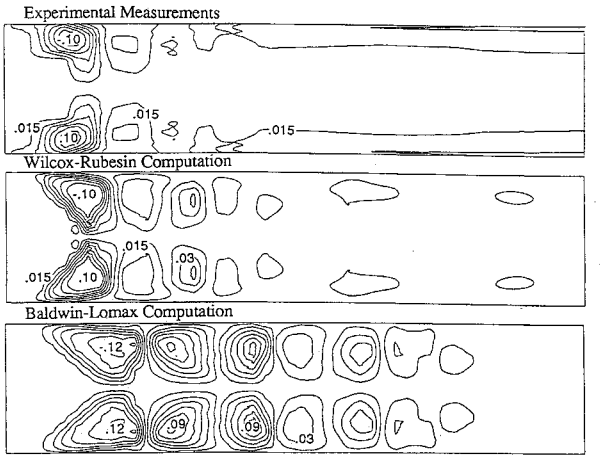

Fig. 4 Transverse velocity contour plots v/U_{ue} shifted for common initial pressure rise; plot range is −0.09 to 0.09 in increments of 0.015, peak values under first shock are labeled.

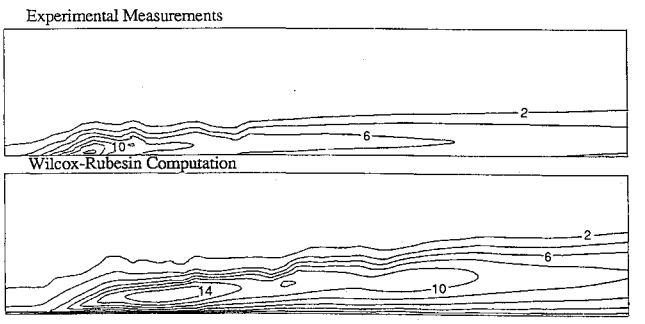

Fig. 5 Turbulence kinetic energy contour plots $k/(U_{ue})^2 \times 10^3$, shifted for common initial pressure rise; plot range is 0.0–16.0 in increments of 2.0.

computation also captures the general features of the transverse velocity distribution, but overpredicts the magnitude of the transverse velocity in the trailing shocks by roughly a factor of six.

Contour plots of turbulence kinetic energy are given in Fig. 5 for the experiments and the Wilcox-Rubesin computation. The Baldwin-Lomax model does not compute this quantity. The freestream turbulence level is nearly zero in both the experiments and computations. A large increase in turbulence kinetic energy occurs at the foot of the first shock, followed downstream by a gradual diffusion in the transverse direction. Good agreement between the computation and the general features of the experiments is observed. However, the computations overpredict the rate of diffusion of turbulence kinetic energy into the core flow and also predict a larger region of elevated turbulence kinetic energy at the foot of the shock than is found experimentally. Peak values of nondimensionalized turbulence kinetic energy at each streamwise location are plotted in Fig. 6. Again, the computed results are shifted such that the initial pressure rise coincides with the experiments. The maximum computed value of $k/(U_{ue})^2$ (U_{ue} is the incoming freestream velocity) occurs slightly downstream of the experimentally determined location, although the magnitude of the computed increase agrees very well with the experimental results. In the later part of the shock train, and in the recovering region downstream, the computation tends to overpredict the level of turbulence kinetic energy. However, it does capture the general trends in this recovery region.

The shifted wall static pressure distributions are shown in Fig. 7. The Wilcox-Rubesin computation shows a more rapid pressure rise than is actually present while the Baldwin-Lomax results have an initially steep pressure rise, then a more gradual downstream pressure increase. The exit pressure imposed in the Wilcox-Rubesin computations was higher than in the experiments. This was done in an effort to properly locate

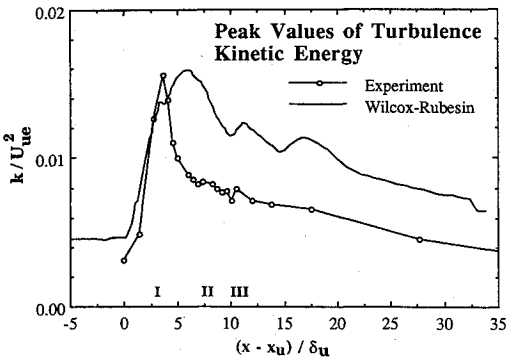

Fig. 6 Distribution of the peak values of turbulence kinetic energy at each streamwise location, shifted for common initial pressure rise. The I, II, and III denote the locations of the first, second, and third shocks, respectively.

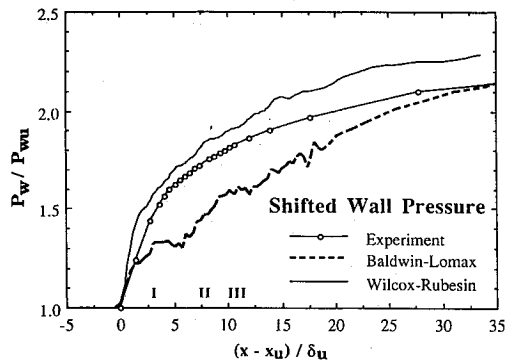

Fig. 7 Wall static pressure distribution, shifted for common initial pressure rise. The I, II, and III denote the locations of the first, second, and third shocks, respectively.

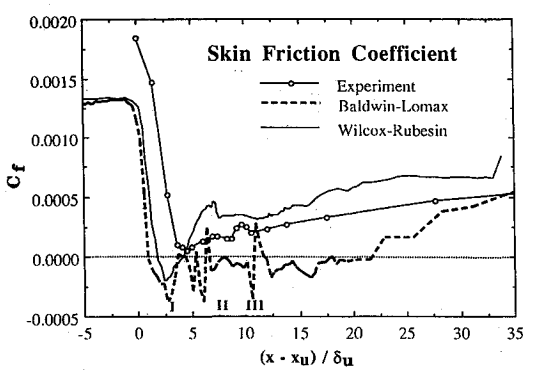

Fig. 8 Skin friction coefficient distribution, shifted for common initial pressure rise. The I, II, and III denote the locations of the first, second, and third shocks, respectively.

the shock train in the duct. The experimental exit pressure level was used for the Baldwin-Lomax case. The major conclusion from this figure is that neither the Wilcox-Rubesin nor the Baldwin-Lomax computations properly predict the magnitude of the wall static pressure rise, even though they do predict the general shape of the pressure rise. Side wall boundary layers are present in the experiment, but were not modeled in the two-dimensional computations. This is consistent with the overprediction of the pressure in the Wilcox-Rubesin computation, but fails to explain the differences in the Baldwin-Lomax computation.

Distributions of the skin friction coefficient are shown in Fig. 8. The experimental values of C_f were obtained from a wall-wake curve fit to the velocity data. Boundary-layer separation was not observed in the experiments. The high confinement levels delay separation until higher Mach numbers than one would expect based on unconfined shock wave/boundary-layer interaction results. Both computations predict boundary-layer separation, with the Baldwin-Lomax computation predicting the largest separated region. Both computations also predict that the minimum skin friction level under the first shock occurs under the bifurcation, while the experiments indicate that it occurs just after the trailing leg of the bifurcation. Close quantitative agreement with the experimental skin friction distribution is not obtained with either turbulence model, and the Baldwin-Lomax calculation does not capture reattachment accurately. It shows erratic behavior over an extended region before final reattachment. The best that can be said is that the computations predict the general trends for the skin friction coefficient and that the Wilcox-Rubesin results come closer to predicting the true level of boundary-layer separation. As noted above, the confining effect of the duct walls tends to decrease the tendency toward separation. The experiments were run in a duct with an aspect ratio (depth-to-height) of 2.4. Even though the experiments were judged to be two-dimensional in the middle 50% of the spanwise direction, the experimental side wall boundary layers may have imposed a slightly higher confinement level than was present in the strictly two-dimensional computations. This may help explain the excessive separation levels in the computations.

Conclusion

The first reported computations that examine in detail the mechanisms in a multiple normal shock wave/turbulent boundary-layer interaction (or shock train) have been presented. The effectiveness of the Baldwin-Lomax algebraic turbulence model and the Wilcox-Rubesin two-equation turbulence model has been evaluated for this flow. The Baldwin-Lomax model failed to accurately capture the shock train flow and showed a higher sensitivity than the Wilcox-Rubesin model to the computational grid. The Wilcox-Rubesin model did a better job of predicting the shock train phenomena and the level of flow separation. It also tended to locate the shock more accurately in the duct. However, the Wilcox-Rubesin model requires significantly more computer resources and is prone to numerical instabilities. The stability problems might be overcome by using a more advanced flow solver, for example a total variation diminishing-type scheme, to mitigate the tendency of the turbulence model equations to go unbounded near the shocks.

Acknowledgments

This work was supported by ONR. Computer time was provided through a grant from the NSF National Center for Supercomputing Applications. Additional support was provided by an ONR Graduate Fellowship for B. F. Carroll.

References

[1]Om, D., Childs, M. E., and Viegas, J. R., "An Experimental Investigation and Numerical Prediction of a Transonic Normal Shock/Turbulent Boundary Layer Interaction," *AIAA Journal*, Vol. 23, No. 5, 1985, pp. 707–714.

[2]Om, D., and Childs, M. E., "An Experimental Investigation of Multiple Shock Wave/Turbulent Boundary Layer Interactions in a Circular Duct," *AIAA Journal*, Vol. 23, No. 10, 1985, pp. 1506–1511.

[3]Carroll, B. F., and Dutton, J. C., "Characteristics of Multiple Shock Wave/Turbulent Boundary Layer Interactions in Rectangular Ducts," *Journal of Propulsion and Power*, Vol. 6, No. 2, 1990, pp. 186–193.

[4]MacCormack, R. W., "The Effect of Viscosity in Hypervelocity Impact Cratering," AIAA Paper 69-354, April 1969.

[5]Wilcox, D. C., and Rubesin, M. W., "Progress in Turbulence Modeling for Complex Flow Fields Including Effects of Compressibility," NASA TP 1517, April 1980.

[6]Baldwin, B. S., and Lomax, H., "Thin Layer Approximation and Algebraic Model for Separated Turbulent Flows," AIAA Paper 78-257, Jan. 1978.

[7]White, M. E., Drummond, J. P., and Kumar, A., "Evolution and Application of CFD Techniques for Scramjet Engine Analysis," *Journal of Propulsion and Power*, Vol. 3, No. 5, 1987, pp. 423–439.

[8]Carroll, B. F., and Dutton, J. C., "Multiple Normal Shock Wave/Turbulent Boundary Layer Interactions," *Journal of Propulsion and Power*, Vol. 8, No. 2, 1992, pp. 441–448.

[9]Carroll, B. F., and Dutton, J. C., "Turbulence Phenomena in a Multiple Normal Shock Wave/Turbulent Boundary Layer Interaction," *AIAA Journal*, Vol. 30, No. 1, 1992, pp. 43–48.

[10]Carroll, B. F., and Dutton, J. C., "Computation of Multiple Normal Shock Wave/Turbulent Boundary Layer Interactions," AIAA Paper 90-2133, July 1990.

[11]Hunter, L. G., and Couch, B. D., "A CFD Study of Precombustion Shock-Trains from Mach 3-6," AIAA Paper 90-2220, July 1990.

[12]Lin, P., Rao, G. V. R., and O'Connor, G. M., "Numerical Investigation on Shock Wave/Boundary-Layer Interactions in a Constant Area Diffuser at Mach 3," AIAA Paper 91-1766, June 1991.

[13]Lin, P., Rao, G. V. R., and O'Connor, G. M., "Numerical Analysis of Normal Shock Train in a Constant Area Isolator," AIAA Paper 91-2162, June 1991.

[14]Liou, M. S., Coakley, T. J., and Bergmann, M. Y., "Numerical Simulation of Transonic Flows in Diffusers," AIAA Paper 81-1240, June 1981.

[15]Viegas, J. R., and Horstman, C. C., "Comparison of Multiequation Turbulence Models for Several Shock Boundary-Layer Interaction Flows," *AIAA Journal*, Vol. 17, No. 8, 1979, pp. 811–820.

[16]Kumar, A., "Numerical Analysis of the Scramjet-Inlet Flow Field by Using Two-Dimensional Navier-Stokes Equations," NASA TP 1940, Dec. 1981.

[17]Kumar, A., "User's Guide for NASCRIN—A Vectorized Code for Calculating Two-Dimensional Supersonic Internal Flow Fields," NASA TM 85708, Feb. 1984.

[18]Knight, D. D., "Improved Calculation of High Speed Inlet Flows. Part II: Results," *AIAA Journal*, Vol. 19, No. 2, 1981, pp. 172–179.

[19]Drummond, J. P., and Weidner, E. H., "Numerical Study of a Scramjet Engine Flowfield," *AIAA Journal*, Vol. 20, No. 9, 1982, pp. 1182–1187.

[20]Coakley, J. R., and Hsieh, T., "A Comparison Between Implicit and Hybrid Methods for the Calculation of Steady and Unsteady Inlet Flows," AIAA Paper 85-1125, July 1985.

[21]Visbal, M., and Knight, D. D., "The Baldwin-Lomax Turbulence Model for Two-Dimensional Shock-Wave/Boundary-Layer Interactions," *AIAA Journal*, Vol. 22, No. 7, 1984, pp. 921–928.

[22]MacCormack, R. W., and Baldwin, B. S., "A Numerical Method for Solving the Navier-Stokes Equations with Application to Shock-Boundary Layer Interactions," AIAA Paper 75-1, Jan. 1975.

[23]Coakley, T. J., and Viegas, J. R., "Turbulence Modeling of Shock Separated Boundary-Layer Flows," *Symposium on Turbulent Shear Flows*, University Park, PA, April 1977.

[24]Viegas, J. R., Rubesin, M. W., and Horstman, C. C., "On the Use of Wall Functions as Boundary Conditions for Two-Dimensional Separated Compressible Flows," AIAA Paper 85-0180, Jan. 1985.

[25]Carroll, B. F., and Dutton, J. C., "A Numerical and Experimental Investigation of Multiple Shock Wave/Turbulent Boundary Layer Interactions in a Rectangular Duct," Dept. of Mechanical and Industrial Engineering, Rept. UILU ENG 88-4015, Univ. of Illinois at Urbana-Champaign, Urbana, IL, Aug. 1988.